Preliminary numerical simulation for the development of a seismic camera

Pedro Matos Casado[1][0000−0001−9328−1769], Emiliano Rustighi[1][0000−0001−9871−7795], Vigilio Fontanari[1][2222−3333−4444−5555], and Jennifer Muggleton[2]

[1] Industrial Engineering Department, University of Trento, Italy
{ph.demelocasadomatos,emiliano.rustighi,vigilio.fontanari}@unitn.it
[2] Institute of Sound and Vibration Research, University of Southampton, UK
jmm@isvr.soton.ac.uk

Abstract. The acoustic camera is an established and highly effective device for localising acoustic sources by the use of a number of simultaneously acquired signals from an array of pressure sensors (microphones). The acoustic camera essentially provides for a highly directional sensor in which the signals arriving from the noise source in the steered main beam of the array are highly amplified relative to the background noise, which arrives at the camera from all directions outside the main beam and is therefore suppressed. The underlying principle of the acoustic camera is the beamforming data processing method which is widely applied in sensor array configurations and acts as a spatial filtering operation. The long term vision of the team is to develop an analogous device, termed here seismic camera, which allow to locate the direction of the noise sources generated from water leaks. This is an array of 3-axis geophones distributed on the ground in the vicinity of the suspected leak to localise and quantify water leaks with significantly greater accuracy and reliability than conventional methods that use just two sensors either side of the leak. The seismic camera differs from the acoustic camera since the array of data is vectorial (three axis geophones provide velocities instead of a scalar pressure field), two or more wave types (compressional, shear and surface waves) propagate simultaneously and the soil properties varies greatly with location, type and condition. In this preliminary feasibility study a time-domain solution calculated from the analytical elasticity equations is considered to generate the numerical data. The wave field is composed by spherical compressional waves radiating directly from the leak which is modelled here as a spherical cavity of radius a. The obtained numerical data is elaborated in order to look at the implementation of the Delay-and-Sum beamforming algorithm for the detection of the leak. Finally, the effects of wave reflection caused by a free surface and the sensor direction of measurement are discussed and it is shown that the beamforming algorithm works better and more precisely in infinity medium models, although the half-space model still presents satisfactory result.

Keywords: water leak source detection · buried pipelines · seismic camera.

1 Introduction

The acoustic camera, often referred to as the acoustic beamforming methods, is a standard method for localising sources of sound waves in free space and has been widely used in different acoustic applications for the past hundred years [1, 2]. The technique is often performed in engineering applications that involves moving objects localisation such as air-crafts, submarines and vehicles and is commonly applied in signals that describes scalar wave fields from pressure fluctuations measurements through microphones. The beamforming algorithms can be interpreted as a spatial filtering operation to map the distribution of sound sources at a certain distance of an array of sensors [2]. However, the technique is yet to be analysed in applications that involves detection of buried sound sources through the use of vector wave field measurements performed by state-measuring sensors such as geophones or accelerometers. Through this approach, the feasibility of the seismic camera and its usage for the localisation of buried leaks in pipes is investigated. The actual state of the art in leak detection is the cross-correlation techniques that involves estimating the leak position [3, 4].

The application of the beamforming method requires prior information on the free-field wave velocity, although this information can either be calculated from theoretical models and ground properties measurements or estimated in-situ with other types of experimental techniques [5]. Zheng et al. [6] applied the beamforming algorithm to estimate the wave speed and then detect leak position along a gas pipeline for different number of sensors. The measurements were made directly on the pipe wall by accelerometers in a no-buried condition. The technique showed good estimates for both the wave velocity and the leak position for all tested cases, although the algorithm required a high computational cost to iterate through the estimates of wave speed and leak position with good resolution. However, no investigation on the beamforming method performance to detect leaks in buried pipes through an array of directional sensors has been made.

The aim of this paper is to investigate the beamforming algorithm performance in detecting a buried noise radiator spatially measured by a geophones array. The analytical solution for the displacements of a spherical wave propagating in an infinite medium is calculated to generate the numerical data. The propagating wave is radiated as an impulse by a symmetrical spherical source of constant radius. As spherical symmetry is assumed, the spatial solution is given only in terms of the radial coordinate which is decomposed in two perpendicular directions to further investigate the effect of the direction of measurement of the wave fields (perpendicular and parallel to the ground surface) and to investigate the method applicability in situations limited by 1D-axis sensors. The infinite medium solution is obtained from the theory of elasticity equations by applying a time pulse in the boundary condition for the radial stress around the spherical source. The half-space medium solution is obtained by considering reflection coefficients and wave mode conversion effects that are calculated from the no-stress boundary conditions at the free-surface. The array of sensors is considered to be a one-dimensional horizontal line of evenly distributed sensors.

A spherical source is placed in any position in relation to any one of the sensors, and the numerical signals are generated from the analytical solutions. At last, the generated data is performed through the Delay-and-Sum beamforming algorithm to generate the signal amplitude map for different trial points in the array surroundings.

The paper is organised as follows. Section 2 presents the beamforming algorithm and review some of its applications. Section 3 presents the propagating spherical wave solution radiated by an impulsive spherical cavity. Then, the formulation that gives the wave reflection coefficients is presented and the expressions for the sensor displacements under reflecting conditions are calculated. Numerical results are presented in Section 4 and the effects of the measurement direction and the reflection on the surface are highlighted. At last, Section 5 presents the concluding remarks of the preliminary study and suggests future analysis.

2 The beamforming algorithm

The beamforming methods refers to a family of array signal processing algorithms that act as a spatial filtering process of the spatially measured signals within an array of sensors. Different variations and strategies of the beamforming algorithm may be found in the literature [2, 7]. Differences between the wide variety of beamforming algorithm strategies include the sensor distribution in the arrays aperture and the deconvolution, inverse and acoustic imaging methods [8]. For a initial feasibility study, the time-domain beamforming Delay-and-Sum algorithm is chosen for the numerical data processing.

The Delay-and-Sum is a simple yet robust beamforming algorithm for source localisation. The algorithm consists in applying a delay to the measured signals of an array and then stacking up the phased signals to obtain an equivalent signal which is amplified in the directions where a source is present. The technique works either if the array is in the far-field or in the near-field with respect to the source, although for the far-field case only the source direction is obtained [2]. Through the delaying process, a main beam of the array is formed and can be mathematically steered acting as if the aperture of the array of sensors was an antenna amplifying signals arriving from sources and suppressing background noise arriving from other directions.

The phase centre is defined as a mean geometric position of the array of sensors, and the time delay applied in each sensors is done in such a way that all the signals would be received there. The distance between the phase-centre and the source trial position is called the main beam of the array. The equivalent signal measured by the phase-centre is mathematically described as [7]

$$z(t) = \Sigma_{m=0}^{M-1} w_m y_m(t - \Delta_m) \tag{1}$$

where M is the number of sensors in the array, w_m is a weight function that is also interpreted as a spatial windowing coefficient useful to relieve spatial aliasing and the leakage effects common to all digital signals, $y_m(t - \Delta_m)$ is the

signal measurement of the m-th sensor which is phased by a time delay of Δ_m. The time delay that phases each sensor depends on the propagating wave, its wave speed and its propagation path. For the case of a spherical wave front, the delay for each sensor can be calculated using the expression

$$\Delta_m = \frac{r^0 - r_m^0}{c_l} \tag{2}$$

where r^0 is the distance between the phase centre and the source trial position, r_m^0 is the distance between the m-th sensor and the source trial position and c_l is the longitudinal wave velocity in the medium. When the source trial position coincides with the source actual position, the signal is amplified to its maximum, pinpointing the noise source location.

3 Elastic Wave Propagation in Free Space

This section presents the solution for the displacements field in an infinite elastic medium given a radial step-pressure stress excitation around a spherical cavity. Moreover, longitudinal incident wave reflection and wave mode conversion on a free-surface are discussed and the amplitude ratio between reflected and incident waves are derived from a no-stress boundary condition at the free-surface.

The analytical solution that generates the numerical data is based on the theory of elasticity which are derived from the stress-strain relationship in a continuous solid and may be rewritten in terms of potentials through the Helmholtz decomposition of a vector quantity. The main assumptions of the formulation are that the solid is elastic, isotropic and continuous and the Lamè constants are the only material properties considered [9]. From this assumptions, it can be shown that two basic wave types can exist in the elastic medium, namely the longitudinal and shear waves. Such waves propagate independently from each other with their own specific velocities that in turn depends only on the medium elastic properties.

The stress equation in terms of the spherical scalar potential ϕ in an infinite medium is given as [9]

$$\tau_{rr} = \lambda \nabla^2 \phi + 2\mu \frac{\partial^2 \phi}{\partial r^2}, \tag{3}$$

where τ_{rr} is the normal stress in the radial direction in $\mathrm{N/m^2}$, λ and μ are the first and second Lamè parameters, both in units of $\mathrm{N/m^2}$, and they are both function of the shear and bulk moduli of the surrounding medium. and ∇ is the space differential vector operator reduced to $\partial/\partial r$ due to the spherical symmetry.

In practical applications the arriving wave fronts detected by the sensors in the array often carry a wide-band frequency energy, and thus, impulse stress boundary condition is considered to obtain the analytical solution that generates the numerical data. The analytical solution for a longitudinal spherical impulse

radiated by a spherical cavity of radius a is obtained by considering the following stress condition around the cavity's surface

$$\tau_{rr}(a, \theta, t) = -p_0 \delta(t), \tag{4}$$

where p_0 is the pressure amplitude in $\mathrm{N/m^2}$ and $\delta(t)$ is the Dirac Delta function. The initial conditions are considered to be homogeneous and are written as $u(r, 0) = \dot{u}(r, 0) = 0$. Also, the spherical symmetry of the problem is exploited so that the displacements are described only in terms of the radial component of the coordinate system. The radial component of the displacement will be further decomposed in two perpendicular directions to simulate the sensor direction of measurement. By applying the stress condition around the cavity in Eq. (4) in Eq. (3), the displacement field for the medium is obtained as

$$u_r(r, \tau) = \frac{1}{r} \frac{a^2}{\rho c_l} \frac{(1-\nu)}{\sqrt{1-2\nu}} \exp(\xi\tau) \left[\left(\frac{1}{r} + \frac{a}{c_l} \right) \sin \omega\tau + \cos \omega\tau \right] \tag{5}$$

where r is the radial distance from the spherical source in metres, τ corresponds to the difference between a reference time and the flight duration of the radiated wave and is related to the position of the wave front for all time. For a pulsating sphere of radius a, the time delay may be written as $\tau = t - (r - a)/c_l$, where c_l is the longitudinal wave speed in m/s. The frequency parameters ξ and ω are function of the medium Poisson's ratio and the source radius and are expressed as $\xi = (1 - 2\nu)c_l/(1 - \nu)a$ and $\omega = \xi(1 - 2\nu)^{-1/2}$.

Fig. 1 illustrates the described model showing a spherical longitudinal wave propagating with velocity c_l. The wave is radiated by a spherical pulsating source and the medium properties are known. When a free-surface is added to the model, both wave reflection and mode conversion may occur. Upon arrival onto the free-surface, the incident wave energy may be distributed between a reflected shear and/or reflected longitudinal wave whose energy distribution depends on the boundary condition and incident angle θ_1.

To calculate the energy distribution between the reflected waves in terms of the reflection coefficients, the free-surface is set to have a no-stress boundary condition. Then the general D'Alambert solution of the wave equation is assumed for the potentials. This is consistent with the impulse formulation since the system is observed to be non-dispersive and thus no distortion of the wave shape occurs. The boundary condition on the free surface is modelled as the no-stress condition and may be expressed as

$$\tau_{yy} = \tau_{yx} = \tau_{yz} = 0. \tag{6}$$

The amplitude ratio between the incident and the reflected waves may be obtained by considering the D'Alambert solution for the scalar and the vector potentials as [9]

$$\phi = A_1 f(k_p(x \sin\theta_1 + y \cos\theta_1 - c_p t)) + A_2 f(k_p(x \sin\theta_1 - y \cos\theta_1 - c_p t)), \tag{7}$$

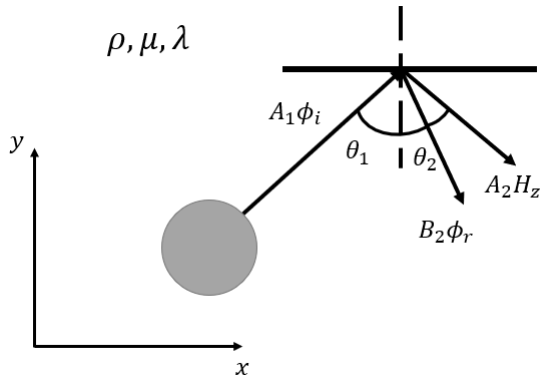

Fig. 1: A compressional wave with amplitude A_1 is emitted by a spherical cavity of radius a and then is reflected upon arrival in the free surface with incidence angle θ_1. Because of wave mode conversion, a shear wave of amplitude B_2 is reflected with reflection angle θ_2 in conjunction with a compressional wave of amplitude A_2 with reflection angle θ_1.

$$H_z = B_2 f(k_s(x\sin(\theta_2) - y\cos(\theta_2) - c_s t)), \tag{8}$$

where k_p and k_s are the compressional and shear wavenumbers respectively in unit of rad/m and θ_1 is the incident and reflection angle for the compressional wave whereas θ_2 is the reflection angle for the shear wave. The angles θ_1 and θ_2 are defined as the angles between the surface normal direction, defined in Fig. 1 as y, and the wave direction of propagation. For the present paper, it is considered that only compressional waves impinge in the surface and thus only the reflected shear waves exist in the solution. Consequently, only the shear amplitude B_2 is considered in Eq. (8). By substituting Eqs. (7)-(8) in Eq. (6), the amplitude ratios between the incident and reflected compressional waves are obtained as

$$\frac{A_2}{A_1} = \frac{\sin 2\theta_1 \sin 2\theta_2 - k^2 \cos^2 2\theta_2}{\sin 2\theta_1 \sin 2\theta_2 + k^2 \cos^2 2\theta_2}, \tag{9}$$

and for shear wave, the amplitude ratio is defined by

$$\frac{B_2}{A_1} = \frac{2\sin 2\theta_1 \cos 2\theta_2}{\sin 2\theta_1 \sin 2\theta_2 + k^2 \cos^2 2\theta_2}. \tag{10}$$

Note that, since the reflection coefficients and purely real, they may be used directly in the displacement equation described in Eq. (5). Therefore, Eqs. (9) and (10) describes how the energy of the incident wave is distributed between the reflected longitudinal and shear waves, respectively. Note that the energy distribution is a function of both the angle of incidence θ_1 and of the medium material properties that appear as k^2 in Eqs (9)-(10) and represents the ratio between the longitudinal and shear wave velocities, i.e., $k = c_l/c_s$. Therefore,

Eqs. (9) and (10) are considered to calculate the reflected waves amplitudes and their contributions for the total displacements.

Through the Helmholtz decomposition, the total displacement in the x and y directions are written in terms of the scalar potential field ϕ which is related to the compressional waves and the vector potential field H_z which is related to the shear waves. The relationship between the potential fields and the displacements may be written as

$$u_x = \frac{\partial \phi}{\partial x} + \frac{\partial H_z}{\partial y}, \qquad u_y = \frac{\partial \phi}{\partial y} - \frac{\partial H_z}{\partial x}. \tag{11}$$

Note that, since shear waves direction of propagation is perpendicular to the particles motion, the horizontal and vertical contributions of the shear wave are inverted in relation to those of the longitudinal wave. This behaviour may also be observed in Eq. (11) in the partial derivatives of the vector potential H_z. Finally, the x and y components of the displacement in the surface of a half-medium are obtained by substituting the D'Alambert solutions in Eqs. (7)-(8) in Eq. (11) as

$$u_x = \sin\theta_1(A_1 u_i + A_2 u_r) + B_2 \cos\theta_2 u_s, \tag{12}$$
$$u_y = \cos\theta_1(A_1 u_i - A_2 u_r) + B_2 \sin\theta_2 u_s, \tag{13}$$

where u_i, u_r and u_s are the radial displacement component of the incident, reflected and converted waves respectively, as shown in Fig. 1.

4 Results and Discussion

The numerical data is generated by the analytical solution of the pressure impulse discussed in Section 3. The array is considered to contain four sensors that measure the displacements in the horizontal and the vertical directions. The vector component along the radial direction is calculated through vector decomposition and summation of the orthogonal measurements. The sensors are distributed in the array one meter apart from each other and a spherical source (magenta circle) with radius of 5 cm is placed in the point (-0.75,-2) of the coordinate system as represented in Fig. 2. The phase-centre is represented as the green dot and the sensors as red dots in Fig. 3. The pressure amplitude of the impulse is of the order of 1 MPa. The soil has properties of 2000 kg/m^3 density and a bulk and shear moduli of 0.053 GPa and 0.02 GPa respectively which results in longitudinal and shear wave speeds of 200 m/s and 100 m/s respectively. The soil properties were chosen based on the typical sand soil properties described in the work presented in [10]. The sensor distribution through the array and the source position were chosen arbitrarily. The source localisation occur by mapping an arbitrary parameter of the algorithm output and for this analysis the maximum absolute value of the output signal was selected to avoid sign problems with the signal phase. At this step of the algorithm implementation, it is necessary to define a grid of possible source positions from which the delay in

Eq. 2 is calculated for each sensor. For the present work, a square grid of a 29x29 trial points distant 0.25 m apart is chosen to calculate the beamforming delay for the sensors. Note that the choice of the distance between the trial points only limits the source location error, thus a 0.25 m precision is satisfactory for the purpose of this paper. Fig. 3 presents the mapping for the source location for the infinite space (left) and the half space (right) cases for the radial (top row), vertical (middle row) and horizontal (bottom row) components.

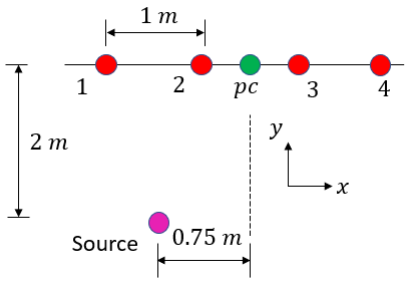

Fig. 2: Schematic representation of the numerical analysis. An array of four sensors (red dot) with the phase centre (green dot) at the origin measures the signal radiated by a spherical source (magenta dot).

A preliminary analysis of Fig. 3 indicates that the beamforming algorithm performance is sensible to the direction of measurement of the signal. Specifically, the horizontal component result in Figs. 3(e) and (f) presents a continuous beam of possible positions for the source location, i.e., the algorithm is only capable of estimating the direction of propagation of the noise. This behaviour is due to the reference frame of the sensors pointing all to the positive x direction of the phase-centre reference point. The reference frame of the sensor defines the sign of the measured signal, thus the number of sensors either side of the source defines the maximum amplitude of the beamforming output. If the number of sensors were equal either side of the leak then the output would be approximately zero and the horizontal coordinate of the source would be defined by a vertical line representing a local minimum of the map. On the other hand, the components r and y were able to pinpoint the source location by the superposition of all the beams formed by the algorithm. As the vertical components of the wave and of the sensors reference frame points to the same direction, no interference occurs and the beamforming output is maximised when the assumed source location coincides with its actual location. Also, it is possible to observe that for the half space results the beam associated with the horizontal direction measurement is reinforced in all directions of measurement along with other minor changes. This effect may be explained by the destructive wave interference caused between the incident and the reflected longitudinal waves, consequently reducing the relative amplitude between the vertical and the horizontal beam-

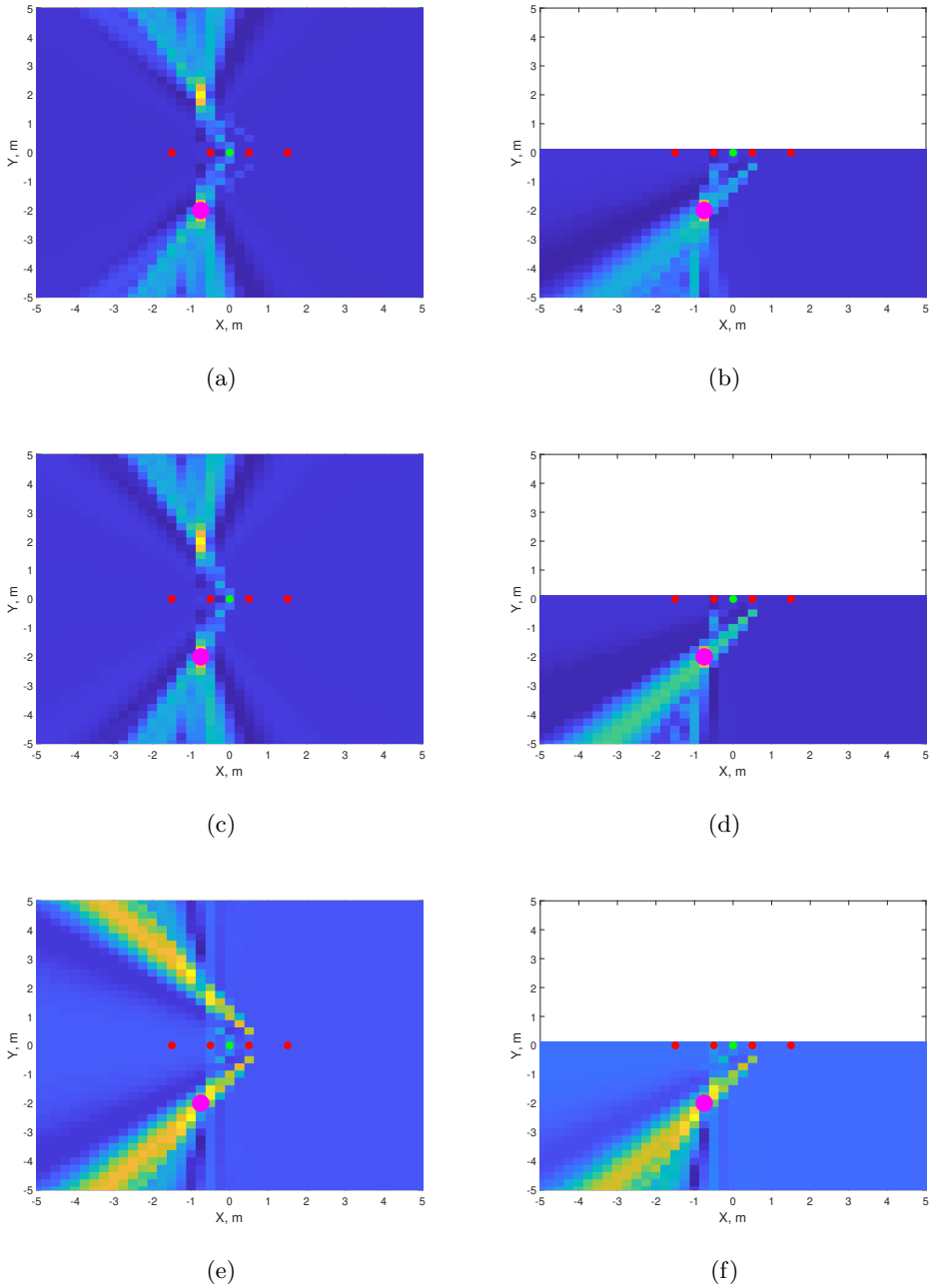

Fig. 3: Source localisation mapping obtained through the application of the beamforming. The left column are the results for the infinite medium and the right column are the results for the half medium. The results are divided by the direction of the components used in the algorithm, where the first row gives the results for the radial component, the middle row for the vertical component and the bottom row for the horizontal component.

forming outputs. In addition, the half-space model considers reflection of shear waves that also contribute for the sensors displacement in both orthogonal directions, thus, depending on the angle of incidence and on the soil properties, the shear displacement contribution in each direction may alter the algorithm mapping.

The results suggest that the infinite medium x-component beamforming simulations may be representative of the half-space results. This possibility may greatly simplify the modelling requirements for more realistic cases and it will also be investigated in future research.

5 Concluding Remarks

The delay-and-sum beamforming technique has been proposed for locating underground sources through an array of directional sensors. A numerical investigation was carried out to analyse the effects of the direction of measurement of the sensor and of the wave reflection on the surface on the algorithm performance. The results for the horizontal direction presented a particular behaviour of estimating only the source direction rather than its approximate location. This behaviour was attributed to the signal cancellation on the x components of the displacements due to the sensors reference frame pointing all to the same direction. In contrast, the results for the vertical and the radial components resulted in the pinpointing of the source location due to the fact that no signal cancelling occurs to signals measured on those directions since the source is located beneath the array. The wave reflection effect did not have much influence on the algorithm performance on locating the source but some output anomalies were observed and correlated to the different contributions of the incident and reflected waves on the signal. In conclusion, the numerical investigation results suggests that the delay-and-sum beamforming algorithm may be a potential alternative technique to remotely locate leaks in buried pipes. Further investigation regarding the beamforming algorithm variants and optimisations are to be carried out in the future, considering more sensors for the array, a more precise model for the wave propagation solution and the effect of the wave velocity estimation on the algorithm performance as well as the soil properties and pressure amplitude effects.

References

1. Ulf Michel. History of acoustic beamforming. In *1st. Berlin Beamforming Conference*, page 18, 2006.
2. Paolo Chiariotti, Milena Martarelli, and Paolo Castellini. Acoustic beamforming for noise source localization – Reviews, methodology and applications. *Mechanical Systems and Signal Processing*, 120:422–448, April 2019.
3. R. Puust, Z. Kapelan, D. A. Savic, and T. Koppel. A review of methods for leakage management in pipe networks. *Urban Water Journal*, 7(1):25–45, February 2010. Publisher: Taylor & Francis.

4. H.V. Fuchs and R. Riehle. Ten years of experience with leak detection by acoustic signal analysis. *Applied Acoustics*, 33(1):1–19, 1991.
5. F.C.L. Almeida, M.J. Brennan, F. Kroll de Lima, M.K. Iwanaga, and O. Scussel. Using a geophone as an actuator to estimate the velocity of leak noise propagation in buried water pipes. *Applied Acoustics*, 184:108251, December 2021.
6. Xiaoliang Zheng, Qiang Wang, Sheng Xue, and Chunshan Zheng. A beamforming-based joint estimation method for gas pipeline leak localization. *Measurement*, 177:109264, June 2021.
7. Don H. Johnson and Dan E. Dudgeon. *Array Signal Processing: Concepts and Techniques*. Prentice Hall, 1992.
8. Q Leclère, A Pereira, C Bailly, J Antoni, and C Picard. A unified formalism for acoustic imaging based on microphone array measurements. *International Journal of Aeroacoustics*, 16(4-5):431–456, July 2017. Publisher: SAGE Publications.
9. Karl F. Graff. *Wave Motion in Elastic Solids*. Dover Publications, April 2012.
10. Yan Gao, Yuyou Liu, and Jennifer M. Muggleton. Axisymmetric fluid-dominated wave in fluid-filled plastic pipes: Loading effects of surrounding elastic medium. *Applied Acoustics*, 116:43–49, January 2017.